Structure Preserving SAR image despeckling via L0-minimization

Gang Liu, Wen Yang, Gui-Song Xia, Ming-Sheng Liao

Machine Copy for Proofreading, Vol. x, y–z, 2013

STRUCTURE PRESERVING SAR IMAGE DESPECKLING VIA $L0$-MINIMIZATION

Gang Liu[1], Wen Yang[1, 2, *], Gui-Song Xia[2], and Mingsheng Liao[2]

[1]School of Electronic Information, Wuhan University, Luo-jia-shan, Wuchang, Wuhan 430072, China

[2]The State Key Laboratory of Information Engineering in Surveying, Mapping and Remote Sensing (LIESMARS), Wuhan University, 129 Luoyu Road, Wuhan 430079, China

Abstract—In this paper, we propose a new method for synthetic aperture radar (SAR) image despeckling via $L0$-minimization strategy, which aims to smooth homogeneous areas while preserve significant structures in SAR images. We argue that the gradients of the despeckled images are sparse and can be pursued by $L0$-norm minimization. We then formularize the despeckling of SAR images as a global $L0$ optimization problem with difference of average operations. Namely, the number of pixels with difference of average that are unequal to one is controlled to approximate prominent structures in a sparsity-control manner. Finally, a numerical algorithm is employed to solve the $L0$ minimization problem. In contrast with existing SAR image despeckling approaches, this strategy is applied without necessity to consider the local features or structures. The performance of our method is tested on high-resolution X-band SAR images. The experimental results show that the proposed method achieves state-of-the-art results in terms of the equivalent-number-of-looks measure and the edge-preserving index.

1. INTRODUCTION

Due to the coherent interference of waves reflected from many elementary scatters, speckle appears in synthetic aperture radar (SAR) images, which degrades the quality of imaging and gives a grainy appearance to the images. Speckle often has a negative effect to the

Received 15 April 2013.

* Corresponding author: Wen Yang (yangwen@whu.edu.cn).

interpretation of SAR images [1, 2]. Thus, despeckling, also known as speckle suppression or filtering, is a major issue in SAR image processing [3–5]. The main goal of despeckling is to remove the speckle effects while preserve structural details, e.g., edges, corners, textures, of the scene. In the past decades, numerous despeckling approaches have been proposed in the literature, most of which are based on the statistics of pixels and the relationship with their surroundings, see [6–8]. However, the hypothetical relationship between pixels is somewhat inaccurate. In addition, pixels even in one image could follow different statistical distributions, which brings difficulties in the estimation parameters [9]. In contrast, we introduce an alternative way for despeckling in this paper, which suppresses speckle by avoiding to model the speckle directly.

The main idea is inspired by the observation that images without speckle (e.g., optical images) are smooth, which implies that the gradients of the despeckled images are sparse. This sparsity can be pursued by $L0$-norm minimization. Compared to $L1$- and $L2$-norm optimization, $L0$-norm optimization has a more sparse solution but has not been solved in closed form so far. Recently, an approximated numerical solution to the $L0$-norm optimization problem was proposed in [10], by relying on a splitting scheme and has been used by Xu et al. [11] for the simplification of nature images. This paper addresses the problem of SAR image despeckling in the context of $L0$-norm minimization. [12] shows that the gradient of SAR images can be well described by the difference of average. Thus, we propose to despeckle an SAR image by minimizing the $L0$-norm of the difference of average of the image. More precisely, combining with a difference of average operator, we introduce a despeckling solution for SAR images based on the mechanism of discretely counting spatial changes. As we shall see, the filtered results will be as smooth as possible in homogeneous areas while the prominent structures, such as edges and point targets, are well preserved. We compare our results with several classic methods, including the improved sigma Lee filter [13], the probabilistic patch-based (PPB) algorithm [7] and the SAR-BM3D algorithm [8].

The rest of the paper is organized as follows. First, some related works are briefly reviewed in Section 2. Then, the difference of average minimization model is described in Section 3 and the solution of the model is introduced in Section 4. Finally, experimental results on SAR images are exhibited in Section 5 and conclusions are drawn in Section 6.

2. RELATED WORKS

In the last several decades, many filtering algorithms have been proposed to deal with the speckle in the analysis of SAR images. These filtering algorithms can be roughly divided into two main categories. The first one resorts to multi-look processing, which is usually adopted during the formation of images. More precisely, in order to reduce speckle, it averages L different looks of the images of the same scene. This process narrows down the probability density function of speckle and reduces the variance by a factor of L. However, it also reduces the ground resolution of the image with proportion of the number of looks. To overcome this problem, an alternative type of approaches has been proposed based on posterior speckle filtering techniques both in frequency domain and in spatial domain [14–16]. Some reviews of the connections and evolutions of the filtering algorithms has been made by [17].

Frequency-domain methods, including both the hard threshold and soft threshold wavelet filtering algorithms, are commonly used for speckle suppression. The main advantage of wavelet transformation is the local description of signal frequency spectrum. Attempts at SAR speckle reduction using wavelet decomposition can resort to logarithm transform. For instance, Foucher et al. proposed a multi-scale filtering method for SAR images by combining the classical adaptive approach with wavelet decomposition. Achim et al. [18] employed the wavelet transformation on the logarithmically transformed SAR images and derived a Bayesian estimator by using an alpha-stable prior distribution. Gleich et al. [19] used the Gaussian Markov random field to model the wavelet coefficients, which can better fit the heave tail property. Most of these methods are based on muti-level pyramidal representation with down-sampling and leads to a serious drawback of which the invariance by translation is not preserved. In order to solve it, the down-sampling procedure should be removed and keep stationary in wavelet transformation [20]. Argenti et al. [21] adopted the undecimated discrete wavelet transform on SAR images and locally adaptive by estimating the mean and variance in each subband. Other works use wavelet transformations with invariant properties for speckle reduction of SAR images include [22, 23]. These methods smoothed the homogeneous areas while preserving strong scatterers and edges, however, they do not work well in the heterogeneous areas: the edges and textures are still blurred in some degree. Additionally, they often suffered from computational cost.

Independently, adaptive spatial filtering is widely used for SAR image denoising. The early algorithms suppress speckles through

an examination of the local statistics surrounding a given pixel using optimization criteria as the local minimum mean square error (LMMSE), for instance, the Lee filter [24], the Frost filter [25], the Kuan filter [26] and their improved version [6, 13]. The gamma-map filter [27] and the refined gamma-map filter [28] later consider both the speckle model and the reflectivity probability density functions. However, the choice of local window size and orientation has a great impact on the performance of these spatial filters. As stated in [29], "*the spatial organization of a surface's reflectance functions is often generated by a number of different processes, each operating at a different scale*". Most of these filters use a local analysis window with fixed size and shape, though adjustable windows of these algorithms for local spatial variations are required. Compared to local filters, non-local algorithms [30], which perform a globally weighted average process to similar pixels, have been widely used for image denoising and reported the state-of-the-art performances. For instance, the probabilistic patch-based (PPB) filter expresses the SAR denoising process as a weighted maximum likelihood estimation problem where the weights are derived in a data-driven way. The SAR-BM3D algorithm [8] despeckles SAR images by combining the concepts of nonlocal filtering and wavelet-domain shrinkage, which has a better capacity to preserve relevant details while smoothing homogeneous areas. However, the smoothing of homogeneous areas and the preserving of edges are still not well balanced in these methods.

The despeckling algorithm we propose in this paper employs a sparse gradient scheme ($L0$-norm for information sparsity pursuit) in a global optimization framework. This method works very well in preserving major edges while smoothing the manageable degree of low-amplitude noise. By taking into account the peculiar features of SAR images, the gradient scheme is implemented by the difference of average operator, when combined with $L0$-minimization. As we shall see, the proposed method exhibits performances comparable or superior to competing techniques on real SAR images. With this method, the follow-up work, such as object extraction [31–34], classification and recognition [35–37], etc., will be easier.

3. SAR IMAGE DESPECKLING WITH $L0$-MINIMIZATION

This section introduces the $L0$-minimization model for despeckling SAR images. First, we briefly recall the $L0$-minimization filtering. Then, we present the SAR image despeckling model via $L0$-minimization with difference of average operations. As we know,

the intensity of SAR image changes rapidly. It differs enormously in different regions, even in adjacent pixels. So the comparison of single pixels appears nonsense and all pixels in one region should be considered. Some classic algorithms calculate the maximization likelihood in a local region to estimate the parameters, such as Lee [6], Kuan [26], etc.. While the proposed algorithm estimates the parameters by comparing regions in a block, using the difference of average of different directions.

3.1. Recall on *L*0-minimization Filtering

Given a discrete image $I : \Omega \mapsto \mathbb{R}$ defined on a grid $\Omega = \{1, 2, \ldots, N\}^2$, let $S : \Omega \mapsto \mathbb{R}$ be the smooth result. Denoting $I(p)$ as the pixel value at the location p, the energy is comprised of a fidelity term and a regularization term, which is defined as

$$E(S) = \sum_{p \in \Omega} \big(I(p) - S(p)\big)^2 + \lambda\, C(S), \tag{1}$$

where $p = (x, y) \in \Omega$ indicates a pixel in the image, $C(S)$ is the $L0$-norm regularization on S and λ is the adjustable weight between the two terms. $C(S)$ can be calculated as follows,

$$C(S) = \#\left\{p \in \Omega;\, |\partial_x S(p)| + |\partial_y S(p)| \neq 0\right\}, \tag{2}$$

which counts all the pixels p in S whose gradient magnitude is nonzero.

This energy function balances the filtering error and the smoothness of the result. Intuitively, the smoother of the result S is, the larger amount of pixels that satisfy the Eq. (2) will be. This method has been reported excellent performances on smoothing images while retaining the major edges [11].

3.2. *L*0-minimization for SAR Image Filtering

As we know, the rapid change of pixels' intensity near the edge and the multiplicative granular noise make the gradient strongly variate in SAR images. However, the difference of average operator has been proved to be efficient in many applications, such as edge detection [12]. The difference of average operator computes the minimal direction of difference of pixels' intensity in one block.

Given an L-look SAR image in intensity format, the intensity I is related to the backscattering coefficient S by following multiplicative model [29]

$$I = S \cdot Z, \tag{3}$$

with Z as random noises with mean $\mathbb{E}(Z) = 1$ and variance $\mathrm{Var}(Z) = \frac{1}{L}$. After a logarithm transform, the multiplicative noise model in Eq. (3) could be turned into an additive noise model,

$$\ln I = \ln S + \ln Z. \tag{4}$$

Thus, the backscattering coefficient S can be estimated by minimizing following energy function,

$$E(S) = \sum_{p\in\Omega} \big(\ln I(p) - \ln S(p)\big)^2 + \lambda\, C(S), \tag{5}$$

with p indicating a pixel in the SAR image. The regularization term $C(S)$ is calculated by employing a difference of average operation.

Split analysis window: Denote $\mathcal{A} = \{-w, \ldots, -1, 0, 1, \ldots, w\}^2$ as an analysis window of given size $(2w+1)^2$, with w as an integer. In order to compute the gradients in different directions, we split $\mathcal{A}$ into different pairwise blocks by a set of lines $\{\ell_i\}_i$,

$$\ell_i(\delta) : (\delta_x, \delta_y) \in \mathcal{A} \mapsto \delta_y = \tan\theta_i \cdot \delta_x, \tag{6}$$

where θ_i is the slant angle of the ℓ_i and we take $\theta_i = \frac{\pi}{8w} \cdot i$ with $i = \{1, \ldots, 4w\}$ in discrete images.

For each direction θ_i, the pair of disjoint blocks are

$$\mathcal{A}_i^+ = \big\{\delta \in \mathcal{A};\, \ell_i(\delta) > 0\big\},$$
$$\mathcal{A}_i^- = \big\{\delta \in \mathcal{A};\, \ell_i(\delta) < 0\big\},$$

as illustrated in Figure 1.

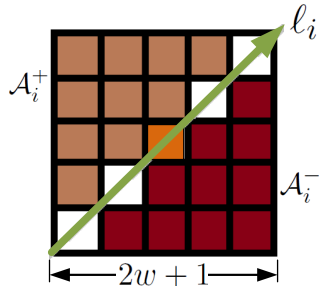

Figure 1. Split analysis window. ℓ_i is denoted as the split line of i-th direction, $\mathcal{A}_i^+$ and $\mathcal{A}_i^-$ are denoted as the two regions on both sides of the split line respectively.

Difference of Average (DoA) operation: For a pixel $p \in \Omega$, the difference between a pair of disjoint image blocks $S(p + \mathcal{A}_i^+)$ and

$S(p+\mathcal{A}_i^-)$ of S with direction θ_i is measured by the difference of average (DoA) of the image blocks as

$$D_i(p) = \left| \langle \ln S(p+\delta) \rangle_{\delta \in \mathcal{A}_i^+} - \langle \ln S(p+\delta) \rangle_{\delta \in \mathcal{A}_i^-} \right|, \tag{7}$$

where $\langle \cdot \rangle_A$ is the arithmetic average operator on the set A. It has been reported that the DoA has the ability to reduce the impaction of speckles [29], which is the main reason to be used for SAR image despeckling.

The gradient $D(p)$ at pixel p is thus taken as the maximal difference of average in all the directions

$$D(p) = \max_{i \in \{1,\ldots,4w\}} D_i(p). \tag{8}$$

Observe that $D(p)$ is much larger than 0 in heterogeneous area and is close to 0 in homogenous areas. The main purpose of this work is to estimate S from I by imposing that $D(p)$ is small in homogenous areas. The half size of the window, w, is a filter parameter and can be empirically set.

So far, the regularization term $C(S)$ in the $L0$-minimization for SAR image filtering can be written as

$$\begin{aligned} C(S) &= \#\{p \in \Omega;\, D(p) \neq 0\} \\ &= \#\{p \in \Omega;\, D_1(p) \neq 0 \text{ or } \ldots \text{ or } D_{4w}(p) \neq 0\}. \end{aligned} \tag{9}$$

with w as the half size of the analysis window.

Remark that the difference of average around one pixel is equal to zero indicates that the block around the pixel is smooth. Instead of considering the pixels' relationship separately, our method takes the block around the pixels as a whole and computes their directional difference. This can eliminate the effects of rapid variations of pixels' intensity.

4. ENERGY MINIMIZATION

This section describes the solution of the proposed $L0$-optimization problem in Eq. (5).

4.1. Computing $C(S)$

Observe that $D_i(p)$ in Eq. (7) can be rewritten as

$$\forall p \in \Omega, \left| \sum_{\delta \in \mathcal{A}_i^+} \ln S(p+\delta) - \sum_{\delta \in \mathcal{A}_i^-} \ln S(p+\delta) \right| \neq 0, \tag{10}$$

which can be implemented by convolving $\ln S$ with a mask filter ϕ_i

$$|\ln S \star \phi_i| \neq 0, \tag{11}$$

with ϕ_i defined by

$$\phi_i(\delta) = \begin{cases} +1 & \text{if } \delta \in \mathcal{A}_i^+ \\ -1 & \text{if } \delta \in \mathcal{A}_i^- \\ 0 & \text{if } \delta \in \mathcal{A} \setminus \mathcal{A}_i^+ \setminus \mathcal{A}_i^- \end{cases} \tag{12}$$

where $\mathcal{A}$ is an analysis window.

Thus, denoting $\Psi_i := \ln S \star \phi_i$, we have

$$C(S) = \# \left\{ p \in \Omega; \sum_{i=1}^{4w} |\Psi_i| \neq 0 \right\}. \tag{13}$$

Integrating Eq. (1), Eq. (4) and Eq. (13), we get the final optimization problem. An explicit solution of this optimization equation is hardly obtained. However, referring to the algorithm in [11], an approximated solution resorting to an iterated procedure is available.

4.2. Two-step Energy Minimization

We use a two-step energy minimization method to solve this problem, in which the auxiliary variables h_i, corresponding to Ψ_i, are introduced to split the object function into two sub-problems [11]. With the auxiliary variables h_i, one can rewrite the objective function as:

$$\min_{S,h_i} \left\{ \sum_{p\in\Omega} \big(\ln S(p) - \ln I(p) \big)^2 + \lambda\, C(h_i) + \beta \sum_{i=1}^{4w} (\Psi_i - h_i)^2 \right\}, \tag{14}$$

where p is the pixel index over the image, $C(h_i) = \#\{p; \sum_{i=1}^{4w} |h_i(p)| \neq 0\}$ and β is an automatically adapting parameter to control the similarity between auxiliary variables h_i and their corresponding Ψ_i. Eq. (14) approaches Eq. (1) when β is large enough. Eq. (14) is decomposed into two parts and solved by alternatively minimization h_i and F. In each iterative procedure, variables are obtained from the previous iteration, and β is augmented for next iteration.

Step 1: computing S. The S estimation subproblem corresponds to minimize

$$E_1 = \sum_{p\in\Omega} \left(\big(\ln S(p) - \ln I(p) \big)^2 + \beta \sum_{i=1}^{4w} \big(\Psi_i(p) - h_i(p) \big)^2 \right), \tag{15}$$

where p is the pixel index over the whole image, by omitting the terms not involving F in Eq. (14). This function is quadratic and has a global minimum [11], which is

$$\widehat{\ln S} = \frac{\widehat{\ln I} + \beta \sum_{i=1}^{4w} \widehat{\phi_i}^* \widehat{h_i}}{1 + \beta \sum_{i=1}^{4w} \widehat{\phi_i}^* \widehat{\phi_i}}, \tag{16}$$

where $\hat{a}$ is the Fourier transform of a and a^* denotes the complex conjugate of a. Observe that it can be implemented using Fast Fourier Transform in $O(2N^2 \log N)$ time complexity, with N^2 as the size of the image.

Step 2: computing h_i. The estimation of h_i is to minimize

$$E_2 = \sum_{p \in \Omega} \sum_{i=1}^{4w} (\Psi_i(p) - h_i(p))^2 + \frac{\lambda}{\beta} C(h_i), \tag{17}$$

with the variable $h_i, i = 1, 2, \ldots, 4w$ and $C(h_i)$ counting the number of non-zero elements in $\sum_{i=1}^{4w} |\Psi_i|$. In this sub-problem, each element $h_i(p)$ is independent of others, so we can estimate them individually with minimizing

$$E_2(p) = \left\{ \sum_{i=1}^{4w} (\Psi_i(p) - h_i(p))^2 + \frac{\lambda}{\beta} H\left(\sum_{i=1}^{4w} |\Psi_i| \right) \right\} \tag{18}$$

where $H(\cdot)$ returns 0 if $\sum_{i=1}^{4w} |\Psi_i| = 0$ and 1 otherwise.

There are two cases in Eq. (18):

(1) when $\sum_{i=1}^{4w} \Psi_i^2(p) \leq \frac{\lambda}{\beta}$,
   - if $h_i(p) = 0, i = 1, \ldots, 4w$, we get $E_2(p) = \sum_{i=1}^{4w} \Psi_i^2(p)$;
   - otherwise, we get $E_2(p) = \sum_{i=1}^{4w} (\Psi_i(p) - h_i(p))^2 + \frac{\lambda}{\beta} \geq \frac{\lambda}{\beta} \geq \sum_{i=1}^{4w} \Psi_i^2(p)$.

   So in this situation, $E_2(p)$ reaches its minimization $\sum_{i=1}^{4w} \Psi_i^2(p)$ at $h_i(p) = 0, i = 1, \ldots, 4w$.

(2) when $\sum_{i=1}^{4w} \Psi_i^2(p) > \frac{\lambda}{\beta}$,
   - if $h_i(p) = 0, i = 1, \ldots, 4w$, we get $E_2(p) = \sum_{i=1}^{4w} \Psi_i^2(p)$;
   - otherwise, $E_2(p)$ reaches its minimization $\frac{\lambda}{\beta}$ at $h_i(p) = \Psi_i(p), i = 1, \ldots, 4w$.

Thus, summing up these points, we get the solution of Eq. (17)

$$\begin{aligned} &(h_1(p), h_2(p), \ldots, h_{4w}(p)) \\ &= \begin{cases} (0, 0, \ldots, 0), & \sum_{i=1}^{4w} \Psi_i(p)^2 \leq \frac{\lambda}{\beta} \\ (\Psi_1(p), \Psi_2(p), \ldots, \Psi_{4w}(p)), & \text{otherwise} \end{cases} \end{aligned} \tag{19}$$

where p indicates the pixels in SAR images.

Our iterative procedure starting with solving h_i via Eq. (19), in which $\beta = \beta_0$ and $\Psi_i = \ln S * \phi_i$. Here β_0 is a small value and F is set to be the original SAR image I. Then h_i is used to solve S via Eq. (16). In next iteration, β is automatically augmented by multiplying κ. The iteration stops on the condition of $\beta > \beta_{\max}$ [11].

Considering that λ changes a lot in different SAR images, we revise it as:

$$\lambda = \Lambda\left(\left\lfloor \lambda' \cdot N^2 \right\rfloor\right),$$

where Λ is the vector storing the pixels' intensity of the original image $\ln I$ in an increasing order, N^2 is the size of the image, $\lfloor a \rfloor$ indicates the largest integer that less than a, and $0 \leq \lambda' \leq 1$ is the new parameter to be tuned (in our experiments, λ' is set to be 0.7).

Algorithm 1 $L0$ difference-of-average SAR image despeckling

Input: SAR image I, filtering weight λ', internal parameters: β_0, $\beta_{\max}$, κ, half patch size w

Output: filtered image S

1: $S^{(0)} \leftarrow I$, $\beta \leftarrow \beta_0$, $j \leftarrow 0$, and obtain λ with Eq. (20);
2: **while** $\beta \leq \beta_{\max}$ **do**
3: solve the auxiliary variables $\{h_i^{(j)}\}_{i=1,\ldots,2W-2}$ with $\Psi_i = \ln S^{(j)} * \phi_i$ and Eq. (19);
4: solve $S^{(j+1)}$ with $\{h_i^{(j)}\}_{i=1,\ldots,2W-2}$ and Eq. (16);
5: $\beta \leftarrow \kappa\beta$, $j \leftarrow j + 1$.
6: **end while**

5. EXPERIMENTS

In this section, we present the experimental results on two scenes of real SAR images, which include plenty of edges and homogenous areas. The *equivalent number of looks* (ENL), the *edge preserved index*(EPI), the *global mean value* [μ] and the *global standard deviation* [σ^2] are used for objective evaluation of the results.

The ENL defined as

$$\mathrm{ENL} = \mu^2/\sigma^2, \tag{20}$$

is a widely used parameter which measures the speckle reduction in homogeneous areas. The larger of the ENL is, the better visual effect the SAR image will have.

The EPI is defined by

$$\mathrm{EPI}=\frac{\sum_{i,j}\sqrt{(p_F(i,j)-p_F(i+1,j))^2+(p_F(i,j)-p_F(i,j+1))^2}}{\sum_{i,j}\sqrt{(p_0(i,j)-p_0(i+1,j))^2+(p_0(i,j)-p_0(i,j+1))^2}}. \quad (21)$$

where p_F denotes the filtered SAR image, p_0 denotes the original SAR image, i, j are the index of the coordinates of the pixels. Contrary to ENL, the EPI is computed in high contrast areas. It evaluates the performance of edge preserving of the tested algorithm. The larger the EPI is, the better performance of the algorithm we can tell.

5.1. Experiment 1

In this experiment, the test image was obtained with the DRA airborne X-band SAR at 3 m resolution, the image size is 538×768 pixels. Figure 2 shows the original SAR image and the corresponding marked regions for performance evaluation. From left to right, the first one in Figure 2 is the original x-band SAR image. The second one shows three homogeneous areas in red boxes, which are used to calculate ENL. The third one shows three heterogeneous areas in green boxes, which are used to calculate EPI. The last one shows three specific areas in yellow boxes, which are used to compare the details. In this experiment, λ is set to be 0.5, β is set to be 1, $\beta_{\max}$ is set to be 2000, κ is set to be 1.8, and the window size of difference computation is set to be 5×5. Our method is compared with Improved Sigma Lee (ImpSigLee), PPB and BM3D, respectively. And the parameters of each algorithm are set to be the best.

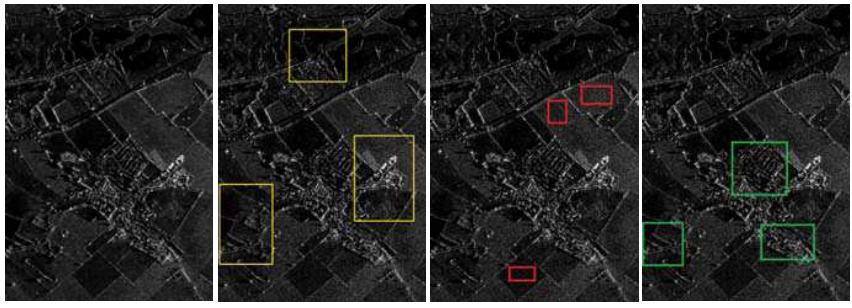

Figure 2. The original image and experimental setup. (a) The original SAR image. (b) Boxes used to calculate ENL. (c) Boxes used to calculate EPI. (d) Boxes used to compare details.

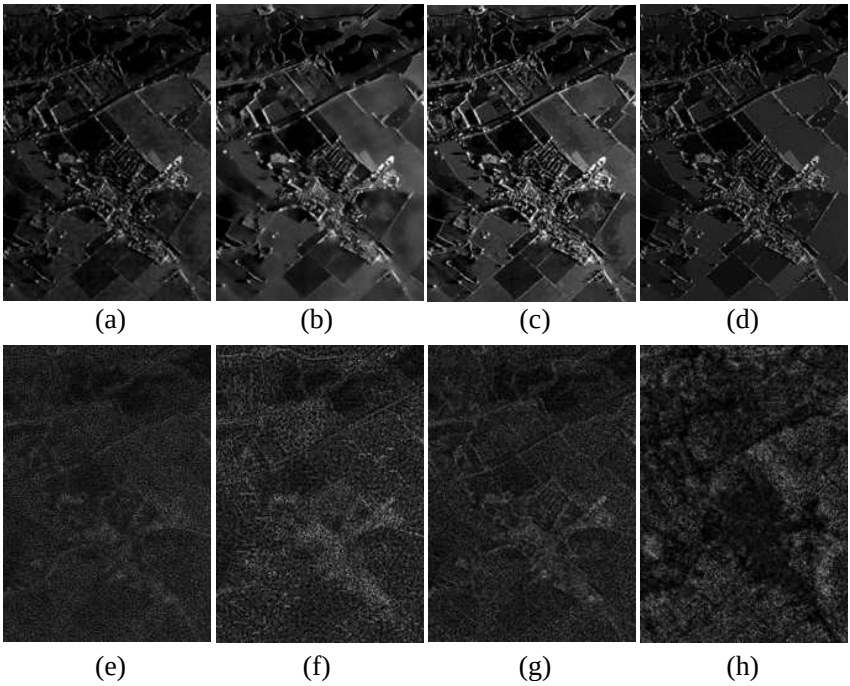

Figure 3. The filtered results of the different methods. (a), (b), (c), (d) Presents the filtered results of Improved Sigma Lee, PPB, BM3D and ours. (e), (f), (g), (h) Presents the difference of filtered SAR image and the original speckled SAR image.

The experimental results are shown in Figure 3 and Figure 4. The upper row of Figure 3 presents the filtered results of Lee, PPB, BM3D and ours. The bottom row of Figure 3 presents the difference of filtered SAR image and the original speckled SAR image. Figure 4 exhibits the details of results, which are chosen from the corresponding SAR image at the same position with yellow boxes in Figure 2. From the first column to the final column, there are the original image details, filtered results of Improved Sigma Lee, PPB, BM3D and ours. We can see that the Improved Sigma Lee filter over smooth the details in the image. PPB performs very well in terms of visual quality. It smoothes the homogenous areas and refines the edges. However, it misses some important point-like targets (Figure 4, block 1 and block 3), edges (Figure 4, block 4), and structures (Figure 4, block 5). Our method could suppress low-amplitude details and enhance high contrast edges to a certain extent. In our result, homogeneous areas are smoothed as

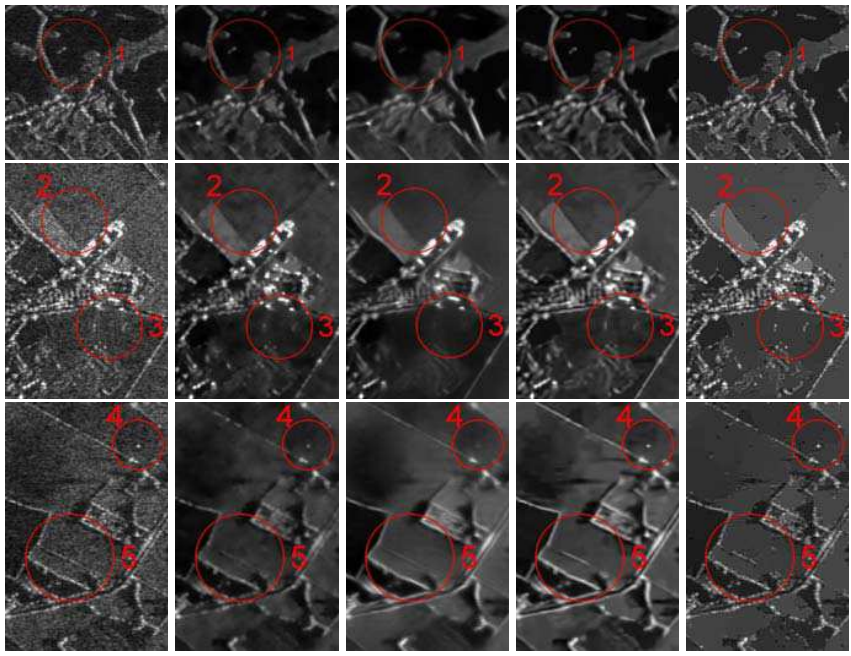

Figure 4. Details of the filtered SAR image. (a) The original image, (b) improved Sigma Lee, (c) PPB, (d) BM3D, and (e) our method.

much as they can, and prominent structures are preserved at the same time. From the analysis of difference images obtained in Figure 3 (i.e., the pointwise difference between the filtered result and the original image. For an ideal filter, the difference image should contain only speckle, the residual of geometric structures or details correlated to the original image indicates that the loss of information of interest), we can find that our result loses the least information of edges and structures.

In order to quantify the performance of our method. We calculated ENL in the red boxes and EPI in the green boxes in corresponding SAR images. The quantified results are given in Table 1, which includes the comparisons of global mean μ, global standard deviation σ^2, ENL and EPI of different filtering methods. From Table 1, we can see that the ENL of Improved Sigma Lee's method is lower than other methods, which explains that the result of Lee filtering is not good from vision. The result of ENL in block 2 of PPB is better than our method, but our result of ENL ranks first in block 1 and block 3. Moreover, the EPI

Table 1. The comparison of global mean, STD, ENL, EPI of different filtering methods.

		Original	ImpSigLee	PPB	BM3D	Ours
Global Mean	-	338.6	**335.8**	341.9	343.9	340.6
Global STD	↓	113.9	86.5	**76.4**	91.5	103.5
Block 1 (ENL)	↑	38.5	492.1	1294.5	674.2	**1988.2**
Block 2 (ENL)	↑	35.4	489.3	**1178.1**	762.4	826.8
Block 3 (ENL)	↑	37.1	641.8	3000.5	965.2	**4412.1**
Block 4 (EPI)	↑	1	0.242	0.169	0.291	**0.974**
Block 5 (EPI)	↑	1	0.218	0.184	0.290	**0.801**
Block 6 (EPI)	↑	1	0.297	0.188	0.292	**0.912**

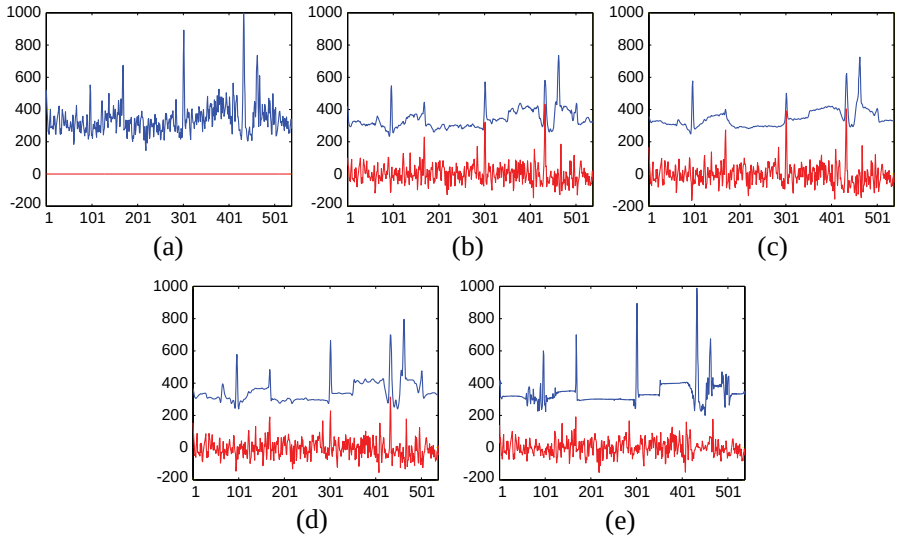

Figure 5. The intensity of one profile in the original and filtered results is presented by blue lines, and the difference of the profile between original and filtered results is presented by red lines. (a) The original image, (b) improved Sigma Lee, (c) PPB, (d) BM3D, and (e) our method.

in three blocks of our method are far better than others because our method enhances the edges by increasing the steepness of transition. Figure 5 is the comparison of intensity of one profile chosen from filtered results of different methods. We can find that the peak of our result is the closest to the original SAR image while the homogenous

area is very smooth except some vibration at intensity transition. The Improved Sigma Lee filter and PPB filter both lose some information about peaks, which is very important in SAR images.

5.2. Experiment 2

In this experiment, we process another scene of X-BAND SAR image, collected by an airborne SAR of China Electronics Technology Group Corporation No. 38 Research Institute, whose spatial resolution is 3 m. The image size is 1467×767 pixels. Figure 6 shows this SAR image and the experimental setup. Similarly, the first one in Figure 6 is the original SAR image. The second one shows three homogeneous areas in red boxes, which are used to calculate ENL. The third one shows two heterogeneous areas in green boxes, which are used to calculate EPI. The last one shows three specific areas in yellow boxes, which are used to compare the details. In this experiment, λ is set to be 0.85, β is set to be 1, $\beta_{\max}$ is set to be 2000, κ is set to be 1.6, and the window size of difference is set to be 7×7. Our method is compared with Improved Sigma Lee, PPB and BM3D, respectively. And the parameters of each algorithm are set to be the best.

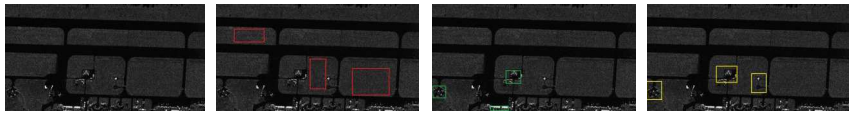

Figure 6. The original image and experiment setup. (a) The original SAR image. (b) Boxes used to calculated ENL. (c) Boxes used to calculated EPI. (d) Boxes used to compare details.

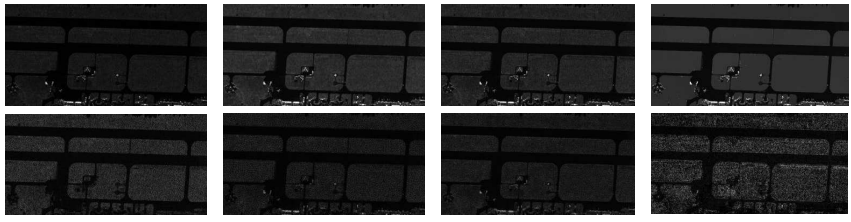

Figure 7. The results of the filtering. (a) The original image, (b) improved Sigma Lee, (c) PPB, (d) BM3D, and (e) our method.

The experimental results are shown in Figure 7 and Figure 8. The

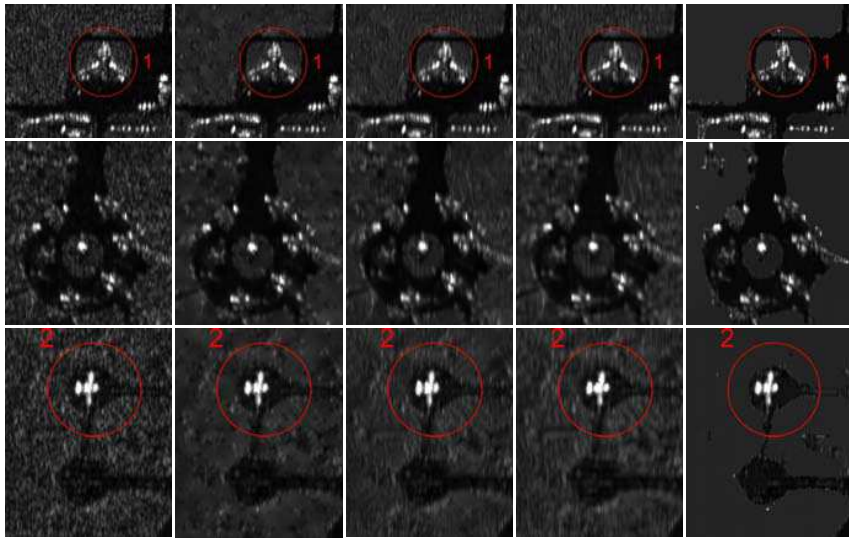

Figure 8. Details of the filtered SAR image. (a) The original image, (b) improved Sigma Lee, (c) PPB, (d) BM3D, and (e) our method.

results of Lee filter is a bit better than the original image from visual interpretation. The result of PPB is better than Improved Sigma Lee because it smoothes the local and refines the edges between different regions to a certain extent. However, in homogenous area the three filters are not smooth enough. Moreover, these methods blur some prominent point-like features (Figure 8, block 1, block 2). In our results, the airplane becomes very prominent and the homogenous areas are also filtered as smooth as possible.

Table 2 demonstrates the comparisons of global mean, global standard deviation, ENL and EPI of different filtering methods in this experiment. From Table 2, we can see that the global mean of our result is very close to the original image. The ENL and EPI of our results are also better than others in most homogenous and high contrast regions respectively, which means that our results have advantages in both homogeneous areas and heterogeneous areas. Figure 9 shows the intensity of one profile in the original and despeckling images, from which we can find that the peaks of our result remain basically unchanged, which is very helpful for preserving the significant structures and edges.

Table 2. The comparison of global mean, STD, ENL, EPI of different filtering methods.

		Original	ImpSigLee	PPB	BM3D	Ours
Global Mean	-	164.6	**163.2**	172.2	170.9	156.7
Global STD	↓	189.4	**179.7**	180.3	180.6	169.1
Block 1 (ENL)	↑	6.553	29.52	25.94	18.18	**520.6**
Block 2 (ENL)	↑	6.221	25.96	21.78	15.94	**97.42**
Block 3 (ENL)	↑	6.884	35.67	29.99	20.00	**1135.3**
Block 4 (EPI)	↑	1	0.787	0.722	0.650	**0.936**
Block 5 (EPI)	↑	1	0.872	0.776	0.705	**1.01**
Block 5 (EPI)	↑	1	**0.990**	0.664	0.573	0.861

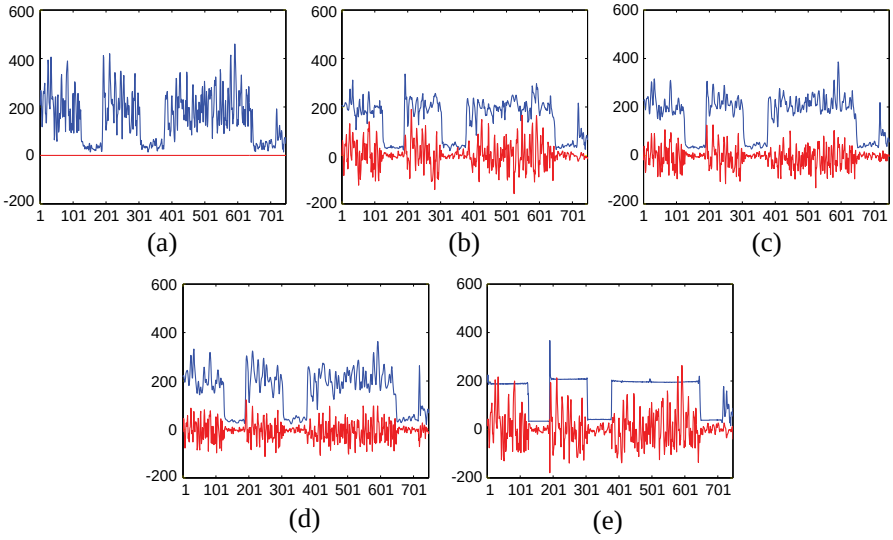

Figure 9. The intensity of one profile in the original and filtered results is presented by blue lines, and the difference of the profile between original and filtered results is presented by red lines. (a) The original image, (b) improved Sigma Lee, (c) PPB, (d) BM3D, and (e) our method.

6. CONCLUSION

In this paper, we have presented a different filtering strategy for SAR images that combines the $L0$ minimization with difference of average operator. Experimental results on real SAR images are encouraging, as

the proposed technique seems to have a better capacity to preserve and enhance the significant structures and edges while extremely smooth the homogenous areas. In other words, it highlights the meaningful structures. With this method, the follow-up work, such as edge detection, object extraction, etc., will be easier.

Examination of local details showed that our method still cannot obtain prefect boundaries in some regions where strong intensity variations span many pixels. One way around this problem would be to adaptive choose the parameter λ according to the heterogeneous degree of different regions in the original SAR images. We intend to explore this option in future work.

ACKNOWLEDGMENT

The research was supported in part by the National Key Basic Research and Development Program of China under Contract 2013CB733404, the Chinese National Natural Sciences Foundation grants (NSFC) 61271401 and the research fund of the Key Laboratory of Geo-informatics of National Administration of Surveying, Mapping and Geoinformation, No. K201203.

REFERENCES

1. Koo, V. C., Y. K. Chan, G. Vetharatnam, M. Y. Chua, C. H. Lim, C.-S. Lim, C. C. Thum, T. S. Lim, Z. Bin Ahmad, K. A. Mahmood, M. H. Bin Shahid, C. Y. Ang, W. Q. Tan, P. N. Tan, K. S. Yee, W. G. Cheaw, H. S. Boey, A. L. Choo, and B. C. Sew, "A new unmanned aerial vehicle synthetic aperture radar for environmental monitoring," *Progress In Electromagnetics Research*, Vol. 122, 245–268, 2012.
2. Fan, C., X.-T. Huang, T. Jin, J.-G. Yang, and D. X. An, "Novel pre-processing techniques for coherence improving in along-track dual-channel low frequency SAR," *Progress In Electromagnetics Research*, Vol. 128, 171–193, 2012.
3. Ren, S., W. Chang, T. Jin, and Z. Wang, "Automated SAR reference image preparation for navigation," *Progress In Electromagnetics Research*, Vol. 121, 535–555, 2011.
4. Li, J., S. Zhang, and J. Chang, "Applications of compressed sensing for multiple transmitters multiple azimuth beams SAR imaging," *Progress In Electromagnetics Research*, Vol. 127, 259–275, 2012.
5. Chen, J., J. Gao, Y. Zhu, W. Yang, and P. Wang, "A novel image

formation algorithm for high-resolution wide-swath spaceborne SAR using compressed sensing on azimuth displacement phase center antenna," *Progress In Electromagnetics Research*, Vol. 125, 527–543, 2012.

6. Lee, J. S., "Refined filtering of image noise using local statistics," *Computer Graphics and Image Processing*, Vol. 15, No. 4, 380–389, 1981.
7. Deledalle, C., L. Denis, and F. Tupin, "Iterative weighted maximum likelihood denoising with probabilistic patch-based weights," *IEEE Trans. on Image Processing*, Vol. 18, No. 12, 2661–2672, 2009.
8. Parrilli, S., M. Poderico, C. Angelino, and L. Verdoliva, "A nonlocal SAR image denoising algorithm based on LLMMSE wavelet shrinkage," *IEEE Trans. on Geoscience and Remote Sensing*, Vol. 50, No. 2, 606–616, 2012.
9. Cheng, J., G. Gao, W. Ding, X. Ku, and J. Sun, "An improved scheme for parameter estimation of G° distribution model in high-resolution SAR images," *Progress In Electromagnetics Research*, Vol. 134, 23–46, 2013.
10. Wang, Y., J. Yang, W. Yin, and Y. Zhang, "A new alternating minimization algorithm for total variation image reconstruction," *SIAM Journal on Imaging Sciences*, Vol. 1, No. 3, 248–272, 2008.
11. Xu, L., C. Lu, Y. Xu, and J. Jia, "Image smoothing via l0 gradient minimization," *ACM Trans. on Graphics*, Vol. 30, No. 6, 174, 2011.
12. Touzi, R., A. Lopes, and P. Bousquet, "A statistical and geometrical edge detector for sar images," *IEEE Trans. on Geoscience and Remote Sensing*, Vol. 26, No. 6, 764–773, 1988.
13. Lee, J. S., J.-H. Wen, T. L. Ainsworth, K.-S. Chen, and A. J. Chen, "Improved sigma filter for speckle filtering of SAR imagery," *IEEE Trans. on Geoscience and Remote Sensing*, Vol. 47, No. 1, 202–213, 2009.
14. Gagnon, L. and A. Jouan, "Speckle filtering of sar images: A comparative study between complex-wavelet-based and standard filters," *SPIE Proceedings, Wavelet Applications in Signal and Image Processing V*, Vol. 3169, 80–87, 1997.
15. Espinoza-Molina, D., D. Gleich, and M. Datcu, "Evaluation of bayesian despeckling and texture extraction methods based on Gauss-Markov and auto-binomial gibbs random fields: Application to TerraSAR-X data," *IEEE Trans. on Geoscience and Remote Sensing*, Vol. 50, No. 5, 2001–2025, 2012.

16. Iqbal, M., J. Chen, W. Yang, P. Wang, and B. Sun, "SAR image despeckling by selective 3D filtering of multiple compressive reconstructed images," *Progress In Electromagnetics Research*, Vol. 134, No. 12, 209–226, 2013.
17. Lee, J. S., L. urkevich, P. Dewaele, P. Wambacq, and A. Oosterlinck, "Speckle filtering of synthetic aperture radar images: A review," *Remote Sensing Reviews*, Vol. 8, No. 4, 313–340, 1994.
18. Achim, A., P. Tsakalides, and A. Bezerianos, "SAR image denoising via bayesian wavelet shrinkage based on heavy-tailed modeling," *IEEE Trans. on Geoscience and Remote Sensing*, Vol. 41, No. 8, 1773–1784, 2003.
19. Gleich, D. and M. Datcu, "Wavelet-based despeckling of SAR images using Gauss-Markov random fields," *IEEE Trans. on Geoscience and Remote Sensing*, Vol. 45, No. 12, 4127–4143, 2007.
20. Shensa, M., "The discrete wavelet transform: Wedding the a trous and mallat algorithms," *IEEE Trans. on Signal Processing*, Vol. 40, No. 10, 2464–2482, 1992.
21. Argenti, F. and L. Alparone, "Speckle removal from SAR images in the undecimated wavelet domain," *IEEE Trans. on Geoscience and Remote Sensing*, Vol. 40, No. 11, 2363–2374, 2002.
22. Sveinsson, J. R. and J. A. Benediktsson, "Almost translation invariant wavelet transformations for speckle reduction of SAR images," *IEEE Trans. on Geoscience and Remote Sensing*, Vol. 41, No. 10, 2404–2408, 2003.
23. Ranjani, J. J. and S. J. Thiruvengadam, "Dual-tree complex wavelet transform based sar despeckling using interscale dependence," *IEEE Trans. on Geoscience and Remote Sensing*, Vol. 48, No. 6, 2723–2731, 2010.
24. Lee, J.-S., "Speckle suppression and analysis for synthetic aperture radar images," *Optical Engineering*, Vol. 25, No. 5, 636–643, 1986.
25. Frost, V., J. Stiles, K. Shanmugan, and J. Holtzman, "A model for radar images and its application to adaptive digital filtering of multiplicative noise," *IEEE Trans. on Pattern Analysis and Machine Intelligence*, Vol. 4, No. 2, 157–166, 1982.
26. Kuan, D., A. Sawchuk, T. Strand, and P. Chavel, "Adaptive noise smoothing filter for images with signal-dependent noise," *IEEE Trans. on Pattern Analysis and Machine Intelligence*, Vol. 7, No. 2, 165–177, 1985.
27. Lopes, A., R. Touzi, and E. Nezry, "Adaptive speckle filters and

scene heterogeneity," *IEEE Trans. on Geoscience and Remote Sensing*, Vol. 28, No. 6, 992–1000, 1990.

28. Baraldi, A. and F. Parmiggiani, "A refined gamma map SAR speckle filter with improved geometrical adaptivity," *IEEE Trans. on Geoscience and Remote Sensing*, Vol. 33, No. 5, 1245–1257, 1995.
29. Xie, H., L. Pierce, and F. Ulaby, "SAR speckle reduction using wavelet denoising and Markov random field modeling," *IEEE Trans. on Geoscience and Remote Sensing*, Vol. 40, No. 10, 2196–2212, 2002.
30. Buades, A., B. Coll, and J. Morel, "A non-local algorithm for image denoising," *Proc. Computer Vision and Pattern Recognition*, Vol. 2, 60–65, 2005.
31. Tian, B., D.-Y. Zhu, and Z.-D. Zhu, "A novel moving target detection approach for dual-channel SAR system," *Progress In Electromagnetics Research*, Vol. 115, 191–206, 2011.
32. Chang, Y.-L., C.-Y. Chiang, and K.-S. Chen, "SAR image simulation with application to target recognition," *Progress In Electromagnetics Research*, Vol. 119, 35–57, 2011.
33. Mohammadpoor, M., R. S. A. Raja Abdullah, A. Ismail, and A. F. Abas, "A circular synthetic aperture radar for on-the-ground object detection," *Progress In Electromagnetics Research*, Vol. 122, 269–292, 2012.
34. Yang, W., Y. Liu, G.-S. Xia, and X. Xu, "Statistical mid-level features for building-up area extraction from full polarimetric SAR imagery," *Progress In Electromagnetics Research*, Vol. 132, 233–254, 2012.
35. Teng, H. T., H.-T. Ewe, and S. L. Tan, "Multifractal dimension and its geometrical terrain properties for classification of multi-band multi-polarized SAR image," *Progress In Electromagnetics Research*, Vol. 104, 221–237, 2010.
36. Park, J.-I. and K.-T. Kim, "A comparative study on ISAR imaging algorithms for radar target identification," *Progress In Electromagnetics Research*, Vol. 108, 155–175, 2010.
37. Jin, Y.-Q., "Polarimetric scattering modeling and information retrieval of SAR remote sensing — A review of FDU work," *Progress In Electromagnetics Research*, Vol. 104, 333–384, 2010.